Free-Energy Barriers of Spin Glasses

E. Bittner, A. Nußbaumer, W. Janke

Free-Energy Barriers of Spin Glasses

Elmar Bittner, Andreas Nußbaumer, and Wolfhard Janke

Institut für Theoretische Physik and Centre for Theoretical Sciences (NTZ), Universität Leipzig
Postfach 100 920, 04009 Leipzig, Germany
E-mail: wolfhard.janke@itp.uni-leipzig.de

The Ising spin glass in the Sherrington-Kirkpatrick (SK) mean field and the three-dimensional Edwards-Anderson (EA) nearest-neighbour formulations are investigated by means of Monte Carlo simulations. To this end, we employ a combination of the multioverlap algorithm with parallel tempering methods. In this report we focus on the finite-size scaling behaviour of the free-energy barriers which are visible in the probability density of the Parisi overlap parameter. Assuming that the mean barrier height diverges with the number of spins N as N^α, our data for the SK model show good agreement with the theoretical prediction $\alpha = 1/3$. We compare the scaling behaviour to the data from the EA model.

1 Introduction

A major open problem in statistical physics is the nature of the "glassy" low-temperature phase of finite-dimensional spin-glass systems. It is still unresolved whether the replica symmetry-breaking theory or the phenomenological droplet picture yields the correct description (for reviews, see Refs. 1–4). Even at the mean-field level, only very recently a mathematical proof[5] of Parisi's replica solution[6] for the Sherrington-Kirkpatrick (SK) model[7] was given.

In the thermodynamic limit the frozen phase of the mean field spin glass shows many stable and metastable states. Such a feature is the consequence of the disorder and the frustration characterising spin glasses in general, leading to a rugged free-energy landscape with probable regions (low free energy) separated by rare-event states (high free energy). But also for finite systems the free-energy landscape shows an intricate, corrugated structure. Therefore, it is hard to measure the free-energy barriers by means of conventional Monte Carlo simulations directly. The aim of this project is to study the free-energy barriers of the SK mean field spin-glass model and the three-dimensional Edwards-Anderson (EA) nearest-neighbour model[8] using a combination of the multioverlap Monte Carlo algorithm[9] with parallel tempering methods[10]. By using this combined algorithm we are able to perform simulations at much lower temperatures for the EA model than in previous studies[11]. This is necessary, because for temperatures close to the spin-glass transition significant deviations from the theoretical mean-field prediction were found in both the three- and four-dimensional EA model. Since one possible explanation for these deviations are strong finite-size effects close to the spin-glass transition, by measuring at lower temperatures these effects should become less pronounced.

2 Model and Simulation Techniques

The Hamiltonian of the Sherrington–Kirkpatrick mean-field model reads

$$H_{\mathrm{SK}} = -\sum_{i<j} J_{ij} s_i s_j \;, \tag{1}$$

where $s_i = \pm 1$, $i = 1,\ldots,N$, with N denoting the number of spins. The exchange coupling constants J_{ij} are quenched, independent random variables with a Gaussian distribution of zero mean and variance N^{-1}. The critical temperature of the infinite system is $T_c = 1$. The SK model gives a mean-field formulation of spin glasses, while the Edwards-Anderson model describes a finite-dimensional spin glass. Here, the sum in the Hamiltonian runs only over nearest-neighbour pairs of Ising spins,

$$H_{\text{EA}} = -\sum_{\langle ij \rangle} J_{ij} s_i s_j \, , \tag{2}$$

where we consider a simple cubic lattice with $N = L^3$ spins and periodic boundary conditions. In the EA model we draw the exchange coupling constants from a symmetric bimodal distribution such that $J_{ij} = \pm 1$, with equal probability. The spin-glass transition temperature in the three-dimensional EA model was found to be $T_c \approx 1.15$.[12]

The fact that there is no explicit order parameter which allows one to exhibit the free-energy barriers led us to use the Parisi overlap parameter[6],

$$q = \frac{1}{N} \sum_{i=1}^{N} s_i^{(1)} s_i^{(2)} \, , \tag{3}$$

where the spin superscripts label two independent (real) replicas for the same realization of randomly chosen exchange coupling constants $\mathcal{J} = \{J_{ij}\}$. For given $\mathcal{J}$ the probability density of q is denoted by $P_{\mathcal{J}}(q)$, and the function $P(q)$ is obtained as

$$P(q) = [P_{\mathcal{J}}(q)]_{\text{av}} = \frac{1}{\#\mathcal{J}} \sum_{\mathcal{J}} P_{\mathcal{J}}(q) \, , \tag{4}$$

where $[\ldots]_{\text{av}}$ symbolises the quenched average and $\#\mathcal{J}$ is the number of realizations considered. For a given realization of $\mathcal{J}$ the nontrivial (i.e., away from $q = \pm 1$) minima are related to the free-energy barriers of this disordered system. We are, therefore, interested in the whole range of the probability density $P_{\mathcal{J}}(q)$. Conventional, canonical Monte Carlo simulations are not suited for such systems because the likelihood to generate the corresponding rare-event configurations in the Gibbs canonical ensemble is very small. This problem can be overcome by non-Boltzmann sampling[13,14] with the multi-overlap weight[9]

$$w_{\mathcal{J}}(q) = \exp\left[\beta \sum_{ij} J_{ij} \left(s_i^{(1)} s_j^{(1)} + s_i^{(2)} s_j^{(2)} \right) + S_{\mathcal{J}}(q) \right] \, , \tag{5}$$

where the sum runs over all pairs of spins for the SK model and only over nearest-neighbour pairs for the EA model. The two replicas are coupled by $S_{\mathcal{J}}(q)$ in such a way that a broad multi-overlap histogram $P_{\mathcal{J}}^{\text{muq}}(q)$ over the entire accessible range $-1 \le q \le 1$ is obtained. When simulating with the multi-overlap weight, canonical expectation values of any quantity $\mathcal{O}$ can be reconstructed by reweighting,

$$\langle \mathcal{O} \rangle_{\mathcal{J}}^{\text{can}} = \langle \mathcal{O} \exp(-S_{\mathcal{J}}) \rangle_{\mathcal{J}} / \langle \exp(-S_{\mathcal{J}}) \rangle_{\mathcal{J}} \, . \tag{6}$$

Ideally the weight function $W_{\mathcal{J}} \equiv \exp(S_{\mathcal{J}})$ should satisfy

$$P_{\mathcal{J}}^{\text{muq}}(q) = P_{\mathcal{J}}^{\text{can}} W_{\mathcal{J}} = \text{const.} \, , \tag{7}$$

i.e., should give rise to a completely flat multi-overlap probability density $P_{\mathcal{J}}^{\mathrm{muq}}(q)$. Of course, $P_{\mathcal{J}}^{\mathrm{can}}(q)$ is a priori unknown and one has to proceed by iteration. An efficient way to construct the weight function $W_{\mathcal{J}}$ is to use an accumulative recursion, in which the new weight factor is computed from all available data accumulated so far[15, 16]. The multi-overlap algorithm combined with this recursion allows an almost automatic simulation.

The efficiency of the multi-overlap algorithm decreases with lowering the temperature, and since we are mainly interested in the low-temperature behaviour of the spin-glass models we had to seek for suitable algorithmic improvements. As a result of this investigation, we developed a combination of the multi-overlap algorithm[9] with the parallel tempering (PT) update scheme[10], where configurations simulated at different temperatures are tried to be exchanged via a Monte Carlo process that typically follows the Metropolis acceptance rules.[17] This renders the combined algorithm particularly suited for a parallel computer such as JUMP at NIC Jülich. For the PT procedure we used a set of N_T temperature values in the range $T_{\min} < T_c < T_{\max}$. Once for each temperature the entire range of q was covered, the accumulative recursion for the weight functions was stopped. Due to large differences in the free-energy landscape for different disorder realizations $\mathcal{J}$, the number of recursion steps varied for different $\mathcal{J}$. After the weight functions were constructed, they were kept fixed and we took our measurements. Thereby, we recorded time series of the overlap parameter q and the canonical $P_{\mathcal{J}}(q)$ distribution for all temperature values, for an EA example see Fig. 1.

3 Analysis Method

To analyse the low temperature behaviour we computed the barrier autocorrelation time τ_B^q for each of these samples $\mathcal{J}$ by employing the same method as Berg *et al.*[11] used for the EA Ising spin-glass model. For clarity, we recall the basic idea here. The free-energy barrier F_B^q for a given $P_{\mathcal{J}}(q)$ is defined through the autocorrelation time of a one-dimensional Markov process which has the canonical $P_{\mathcal{J}}(q)$ distribution as equilibrium state. The transition probabilities $T_{i,j}$ are given by

$$T = \begin{bmatrix} 1 - w_{2,1} & w_{1,2} & 0 & \cdots \\ w_{2,1} & 1 - w_{1,2} - w_{3,2} & w_{2,3} & \cdots \\ 0 & w_{3,2} & 1 - w_{2,3} - w_{4,3} & \cdots \\ 0 & 0 & w_{4,3} & \cdots \\ \vdots & \vdots & \vdots & \ddots \end{bmatrix} , \qquad (8)$$

where $w_{i,j}$ $(i \neq j)$ is a probability à la Metropolis to jump from state $q = q_j$ to $q = q_i$ $(q_i = i/N, i \in [-N, -N+2, \ldots, +N])$,

$$w_{i,j} = \frac{1}{2} \min\left(1, \frac{P_{\mathcal{J}}(q_i)}{P_{\mathcal{J}}(q_j)}\right) . \qquad (9)$$

The transition matrix T fulfills the detailed balance condition (with $P_{\mathcal{J}}$), and as a consequence it has only real eigenvalues. The largest eigenvalue (equal to one) is non-degenerate, and the second largest eigenvalue λ_1 determines the autocorrelation time of the Markov chain,

$$\tau_B^q = -\frac{1}{N \log(\lambda_1)} . \qquad (10)$$

The associated free-energy barrier for realization $\mathcal{J}$ is defined as

$$F_B^q = \ln(\tau_B^q) . \tag{11}$$

Note that the definition of the autocorrelation time (10) takes only barriers in q into account, but not other barriers which may well exist in the multidimensional configuration space.

4   Numerical Details and Results

Let us start with the SK model where we studied systems with $N = 32, 64, 128, 256, 512$, and 1024 spins and used a set of 32 temperature values in the range $T = 1/3 - 1.6$ for all of our systems apart from the largest, where we used 64 temperature values for the same temperature interval. We took about $100\,000$ measurements, with five sweeps between the measurements. A sweep consisted of N spin flips with the multioverlap algorithm and one parallel tempering update. To average over the disorder we used 1000 realizations of the disorder for $N \leq 512$ and 100 for $N = 1024$.

For the EA model we studied systems with $N = 4^3, 6^3, 8^3, 10^3$, and 12^3 spins within a temperature range of $T = 0.5 - 1.5$. Up to $N = 10^3$ we used 11 equally spaced temperature values and for the largest system the spacing below $T = 1$ was halved, leading to 16 replicas. Due to the larger autocorrelation times for the EA model we took at least 10^7 measurements and for the disorder average we used more than 1000 realizations.

For each temperature value we performed least-squares fits of the finite-size scaling (FSS) ansatz $F_B^q = cN^\alpha$ which corresponds to the exponential FSS behaviour

$$\tau_B^q \propto e^{cN^\alpha} . \tag{12}$$

The results for the SK model[18] depicted in Fig. 2 are consistent with previous results in the literature[19–26] using analytical and different numerical methods. The horizontal line in Fig. 2 indicates the theoretical prediction $\alpha = 1/3$ of Ref. 24. The figure shows fits with different lower bounds $N_{\min}$ of the fit range, while the upper bound was always our largest system $N = 1024$. From these fits we observe a strong finite-size effect for $T \to T_c = 1$. At lower temperatures we find a linearly increasing deviation from the theoretical value. This is presumably also a finite-size effect, because the slope of the deviation becomes flatter when increasing the lower bound of the fit range and there is no physical reason for a change of behaviour of the barrier autocorrelation time in the glassy phase. Using ansatz (12) for the EA model, the value of the exponent α varies from 0.49 to 0.46 in the interval $T_c \geq T \geq 0.8$, but the quality of the fits is unacceptably low. Only for the smallest temperatures the goodness-of-fit parameter Q is significantly larger then zero, c.f. Fig. 2. We therefore performed power-law fits as in Ref. 11,

$$\tau_B^q = cN^\alpha, \tag{13}$$

which corresponds to a fit of the form $F_B^q = \log(c) + \alpha \log(N)$. The Q-values for these fits are much closer to unity, see Fig. 2. Our data favour them strongly over the exponential finite-size scaling behaviour (12), which confirms previous results[11] for $T = 1$ and extends them to considerably lower temperatures.

One possible explanation for this deviation from the theoretical value is the lack of self-averaging of the finite volume Parisi overlap parameter distribution $P_{\mathcal{J}}$ in the SK model.[27] This has been confirmed numerically for the SK model[18] as well as for the EA model[11].
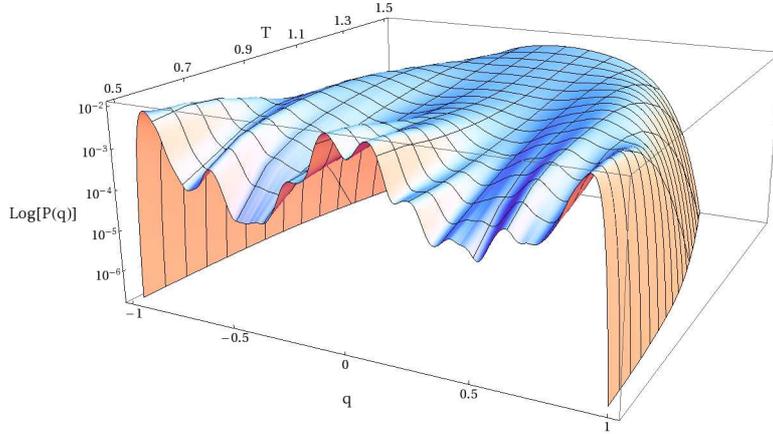
Figure 1. EA model: The logarithm of the canonical $P(q)$ distribution for a 8^3 lattice as a function of temperature for a typical disorder realisation.
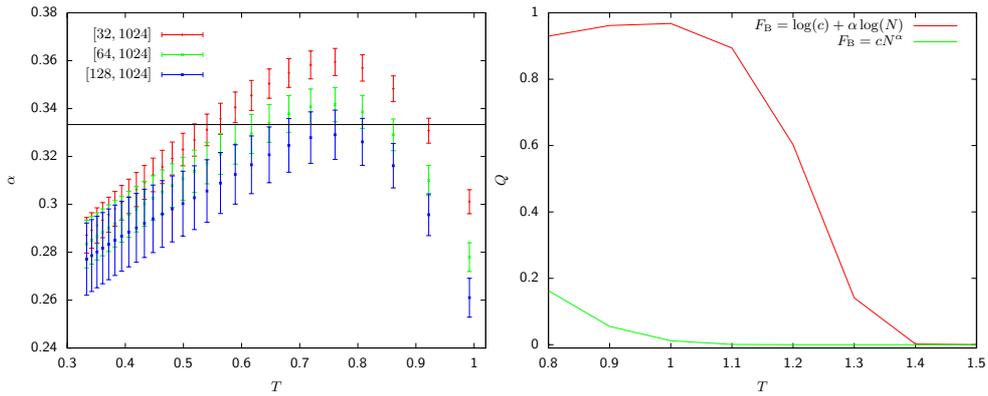
Figure 2. SK model (left plot): Dependence of the exponent α on the lower bound of the fit range $[N_{\min}, 1024]$ as a function of temperature. The horizontal line indicates the theoretical value $\alpha = 1/3$. EA model (right plot): Goodness-of-fit parameter Q as a function of temperature for different types of fits.

We already mentioned that the distribution of the free-energy barriers becomes broader for low temperatures. In recent work Dayal *et al.* have found that the tunnelling times of their flat-histogram sampling simulations of the 2D $\pm J$ Ising spin glass are distributed according to the Fréchet extreme-value distribution for fat-tailed distributions.[28] In general, extreme-value statistics can be classified into different universality classes[29,30], depending on whether the tails of the original distribution are fat tailed (algebraic), exponential, or thin tailed (decaying faster then exponential). Assuming that the tunnelling times respectively free-energy barriers are distributed according to an extreme-value distribution, we use the
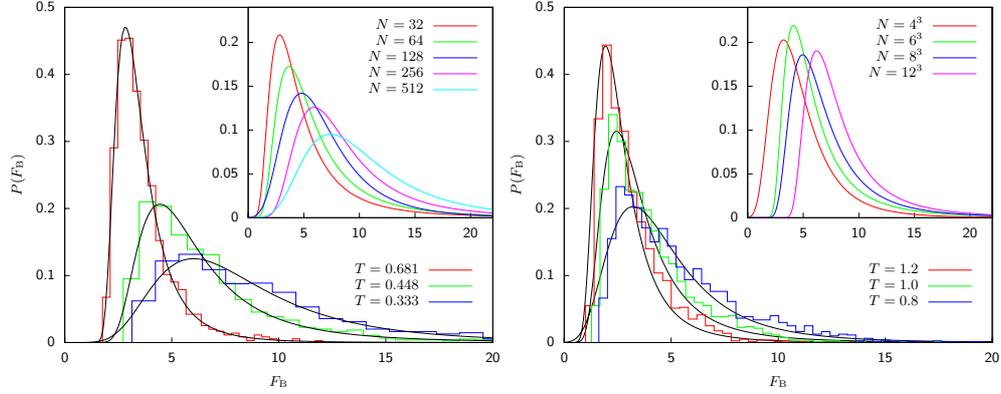
Figure 3. SK model (left plot): Distribution of free-energy barriers F_B^q for $N = 256$ at different temperatures. The inset shows the distribution for $T = 1/3$ for different numbers of spins. EA model (right plot): The same graph as for the SK model for $N = 4^3$ at different temperatures and the inset shows the distribution for $T = 0.8$ for different lattice sizes.

integrated probability density of the generalized extreme-value distribution (GEV),

$$F_{\xi;\,\mu;\,\sigma}(x) = \exp\left[-\left(1 + \xi\frac{x - \mu}{\sigma}\right)^{-1/\xi}\right] \tag{14}$$

for $1 + \xi(x - \mu)/\sigma > 0$, to fit our data. We find that the free-energy barriers show fat tails for $T < T_c$ with shape parameter $\xi > 0$, i.e., a Fréchet distribution. In Fig. 3 we plot the resulting distribution for the SK model for different temperatures below the spin-glass transition and find that the tails become fatter and fatter as the temperature goes to zero. The histograms for low temperatures show deviations from the Fréchet distribution for small values of F_B^q, so a much larger number of disorder realizations would be needed to determine both tails of the distribution properly. We determined the parameters σ, μ and ξ for different temperatures and found that σ grows linearly and μ logarithmically with inverse temperature $1/T$, whereas ξ stays more or less constant at $\xi \approx 0.33$. As an example we show in Fig. 4 the results for $N = 512$. If we keep the temperature fixed and look at the size dependence of the distribution, we find that for a larger number of spins the distribution becomes broader, c.f. the inset of Fig. 3. To quantify this behaviour we use the scaling relations $\sigma \propto N^{\alpha(\sigma)}$ and $\mu \propto N^{\alpha(\mu)}$, which lead to $\alpha(\sigma) \approx 0.25$ and $\alpha(\mu) \approx 0.31$ for our lowest temperatures, see the inset of Fig. 4. We find a temperature dependence of the exponents $\alpha(\sigma)$ and $\alpha(\mu)$ with negative and positive slope for increasing T, respectively. For the EA model we also find fat-tailed distributions, but the broadening of the distribution with increasing number of spins is much weaker than for the SK model, see Fig. 3.

5 Conclusion

We found that the free-energy barriers of the SK model are non-self-averaging and distributed according to the Fréchet extreme-value distribution. These particular features were
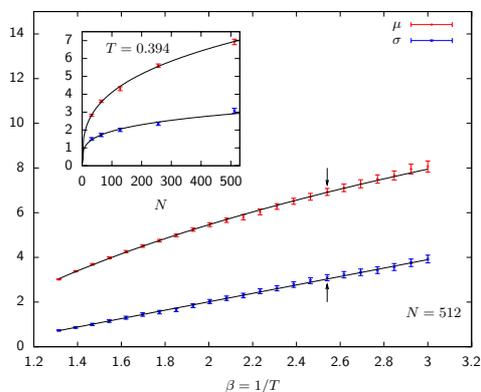
Figure 4. SK model: Temperature dependence of the parameters σ and μ of the Fréchet distribution for $N = 512$. The inset shows the size dependence of σ and μ for $T = 0.394$, indicated by the arrows.

also found for the EA nearest-neighbour model and such similarities support the position that the Parisi replica symmetry breaking solution of the SK model is the limit of the short-range model on a lattice in dimension d when $d \rightarrow \infty$, with a proper rescaling of the strength of the Hamiltonian. On the other hand, we also found that the free-energy barriers diverge with the theoretically predicted value $\alpha = 1/3$, which is in contrast to our results for the EA model in three dimensions and previous findings for the three- and four-dimensional EA model[11].

Acknowledgments

References

1. A.P. Young (ed.), *Spin Glasses and Random Fields* (World Scientific, Singapore, 1997).
2. K.H. Fischer and J.A. Hertz, *Spin Glasses* (Cambridge University Press, Cambridge, England, 1991).
3. M. Mezard, G. Parisi, and M.A. Virasoro, *Spin Glass Theory and Beyond* (World Scientific, Singapore, 1987).
4. K. Binder and A.P. Young, Rev. Mod. Phys. **58** (1986) 801.
5. M. Talagrand, C. R. Acad. Sci. Paris, Ser. I **337** (2003) 111.

6. G. Parisi, Phys. Rev. Lett. **43** (1979) 1754.

7. D. Sherrington and S. Kirkpartick, Phys. Rev. Lett. **35** (1975) 1792.

8. S. F. Edwards and P. W. Anderson, J. Phys. F: Metal Phys. **5** (1975) 965.

9. B.A. Berg and W. Janke, Phys. Rev. Lett. **80** (1998) 4771.

10. K. Hukushima and K. Nemoto, J. Phys. Soc. Jpn. **65** (1996) 1604.

11. B.A. Berg, A. Billoire, and W. Janke, Phys. Rev. B **61** (2000) 12143.

12. M. Palassini and S. Caracciolo, Phys. Rev. Lett. **82** (1999) 5128; H.G. Ballesteros, A. Cruz, L.A. Fernandez, V. Martin-Mayor, J. Pech, J.J. Ruiz-Lorenzo, A. Tarancon, P. Tellez, C.L. Ullod, and C. Ungil, Phys. Rev. B **62** (2000) 14237; M. Pleimling and I.A. Campbell, Phys. Rev. B **72** (2005) 184429.

13. B.A. Berg, Fields Inst. Commun. **26** (2000) 1.

14. W. Janke, Physica A **254** (1998) 164.

15. B.A. Berg, J. Stat. Phys. **82** (1996) 323.

16. W. Janke, *Histograms and All That*, in: *Computer Simulations of Surfaces and Interfaces*, NATO Science Series, II. Mathematics, Physics and Chemistry, Vol. **114**, eds. B. Dünweg, D.P. Landau, and A.I. Milchev (Kluwer, Dordrecht, 2003); p. 137.

17. N. Metropolis, A.W. Rosenbluth, M.N. Rosenbluth, A.H. Teller, and E. Teller, J. Chem. Phys. **21** (1953) 1087.

18. E. Bittner and W. Janke, Europhys. Lett. **74** (2006) 195.

19. N.D. Mackenzie and A.P. Young, Phys. Rev. Lett. **49** (1982) 301; J. Phys. C: Solid State Phys. **16** (1983) 5321.

20. K. Nemoto, J. Phys. A: Math. Gen. **21** (1988) L287.

21. G.J. Rodgers and M.A. Moore, J. Phys. A: Math. Gen. **22** (1989) 1085.

22. D. Vertechi and M.A. Virasoro, J. Phys. (France) **50** (1989) 2325; Europhys. Lett. **12** (1990) 589.

23. S.G.W. Colborne, J. Phys. A: Math. Gen. **23** (1990) 4013.

24. H. Kinzelbach and H. Horner, Z. Phys. B **84** (1991) 95.

25. H. Takayama, H. Yoshino, and K. Hukushima, J. Phys. A: Math. Gen. **30** (1997) 3891.

26. A. Billoire and E. Marinari, J. Phys. A: Math. Gen. **34** (2001) L727.

27. L.A. Pastur and M.V. Shcherbina, J. Stat. Phys. **62** (1992) 1.

28. P. Dayal, S. Trebst, S. Wessel, D. Würtz, M. Troyer, S. Sabhapandit, and S.N. Coppersmith, Phys. Rev. Lett. **92** (2004) 097201.

29. E.J. Gumbel, *Statistics of Extremes* (Columbia University Press, New York, 1958).

30. J. Galambos, *The Asymptotic Theory of Extreme Order Statistics*, 2nd ed. (Krieger Publishing, Malibar, Florida, 1987).